Tissue and Cell 73 (2021) 101653

Contents lists available at ScienceDirect

Tissue and Cell

journal homepage: www.elsevier.com/locate/tice

Automatic segmentation of blood cells from microscopic slides: A comparative analysis

Deponker Sarker Depto [a], Shazidur Rahman [a], Md. Mekayel Hosen [a], Mst Shapna Akter [a], Tamanna Rahman Reme [a], Aimon Rahman [a], Hasib Zunair [b], M. Sohel Rahman [c], M.R. C. Mahdy [a,*]

[a] Department of Electrical & Computer Engineering, North South University, Bashundhara, Dhaka, 1229, Bangladesh
[b] Concordia University, Montreal, QC, Canada
[c] Department of Computer Science & Engineering, Bangladesh University of Engineering and Technology, ECE Building, West Palasi, Dhaka, 1205, Bangladesh

ARTICLE INFO

Keywords:
Blood-cell segmentation
Benchmark
Microscopy data
Deep learning

ABSTRACT

With the recent developments in deep learning, automatic cell segmentation from images of microscopic examination slides seems to be a solved problem as recent methods have achieved comparable results on existing benchmark datasets. However, most of the existing cell segmentation benchmark datasets either contain a single cell type, few instances of the cells, not publicly available. Therefore, it is unclear whether the performance improvements can generalize on more diverse datasets. In this paper, we present a large and diverse cell segmentation dataset BBBC041Seg[1], which consists both of uninfected cells (i.e., red blood cells/RBCs, leukocytes) and infected cells (i.e., gametocytes, rings, trophozoites, and schizonts). Additionally, all cell types do not have equal instances, which encourages researchers to develop algorithms for learning from imbalanced classes in a few shot learning paradigm. Furthermore, we conduct a comparative study using both classical rule-based and recent deep learning state-of-the-art (SOTA) methods for automatic cell segmentation and provide them as strong baselines. We believe the introduction of BBBC041Seg will promote future research towards clinically applicable cell segmentation methods from microscopic examinations, which can be later used for downstream tasks such as detecting hematological diseases (i.e., malaria).

1. Introduction

Peripheral blood examination to identify hematological diseases remains as one of the low-cost and essential diagnosis processes (Nierhaus et al., 2013). Manual examination of microscopic slides heavily relies on the expertise of the examiner. Heavy workloads and insufficient training can cause misdiagnosis, which has motivated researchers to automate the diagnosis process. However, more focus has been given to the identification of the cell types, which can help in making a diagnosis. A practical use-case for the identification of cell types is done in two stages. First, each of the cells is segmented from the microscopic or peripheral examination in blood patches. This is followed by identifying the cell type of each of the individual blood patches. Cell counting is another crucial matter as the number of blood cells in-dicates the presence of specific diseases, and segmentation is essential for cell counting (Hamouda et al., 2012; Alomari et al., 2014; Ghosh et al., 2016; Moallem et al., 2017).

Even though there exist methods for cell segmentation with remarkable results, they are not validated on large enough data-sets. Furthermore, the generalization ability of the methods remains confined in a limited scope due to single cell types. This is problematic as blood cells, particularly red blood cells, can have numerous morphological differences (Ford, 2013). Hence, datasets containing only biconcave disk-shaped RBC cells are not enough to ensure a particular method that is tested thereon. Cell segmentation methods would fail in real-world scenarios, such as overlapping of cells, staining, and slide preparation differences if these are not represented in the datasets used for these tasks. With this backdrop, in this paper, we conduct extensive

* Corresponding author.
E-mail addresses: deponker.sarker@northsouth.edu (D.S. Depto), shazidur.rahman@northsouth.edu (S. Rahman), mekayel.hosen@northsouth.edu (Md.M. Hosen), shapna.akter@northsouth.edu (M.S. Akter), rahman.reme@northsouth.edu (T.R. Reme), aimon.rahman@northsouth.edu (A. Rahman), hasibzunair@gmail.com (H. Zunair), msrahman@cse.buet.ac.bd (M.S. Rahman), mahdy.chowdhury@northsouth.edu (M.R.C. Mahdy).
[1] https://github.com/Deponker/Blood-cell-segmentation-dataset

https://doi.org/10.1016/j.tice.2021.101653
Received 11 June 2021; Received in revised form 2 September 2021; Accepted 15 September 2021
Available online 17 September 2021

experimentation considering both learning and non-learning-based algorithms for documenting baseline performances in a large manually annotated blood cell segmentation dataset. Hence, we benchmarked widely accepted algorithms in medical image analysis for microscopic cell segmentation and provided important insights regarding their performances on the proposed dataset. To this end, this is expected to be a benchmark study for future research on this topic.

1.1. Cell segmentation methods

1.1.1. Non-learning based methods

Several rule-based image processing techniques have been widely used over the years to segment blood cells from microscopic slides. Among the most commonly used algorithms, there is color-based segmentation, where dominant hue range with calculated optimal saturation thresholds in HSV color space is used to segment red blood cells and parasites from images (Makkapati and Rao, 2009). A normalized cut method has been implemented in RGB, YCbCr, HSV, and NTSC using Rands Index (Mandal et al., 2010). K-mean clustering segments images by creating multiple disjoint subsets equal to K from provided blood cell images and defines unique centroids for each subset (Savkare et al., 2016; Nasir et al., 2012; Mohapatra et al., 2011; Ghane et al., 2017; Zhang et al., 2014; Savkare and Narote, 2015). The watershed treats pixel values as local topography and floods basins from user-defined markers until different markers meet on watershed lines (Sharif et al., 2012; Algailani and Hamad, 2018; Sundara and Aarthi, 2019; Mohammed et al., 2013; Jiang et al., 2003). Thresholding techniques include Otsu's method, which determines an optimal intensity threshold that separates image pixels into foreground and background (Nawa et al., 2019). Thresholding and canny edge detector segments images utilizing boundary-based methods and morphological operations enhance the local and global details of the output (Al-Hafiz et al., 2018; Madhloom et al., 2012; Liao and Deng, 2002; Sadeghian et al., 2009). Contour-related methods include a model-based contour identification approach to automatically segment images of red blood cells (Vromen and McCane, 2006) and Hausdorff dimension jointly with contour signature for classifying cell nucleus in fuzzy clustering-based two-stage color segmentation method (Mohapatra et al., 2010).

1.1.2. Learning based methods

Sheng et al. (2020) implemented a CNN followed by a Region Proposal Network (RPN) and fully connected (FC) layer to determine the cell classes and identification of boundary boxes. Ma et al. (2020) implemented DCGAN followed by ResNet that classifies 4 types of WBCs. Other methods also involve pre-trained AlexNet with modifications in the last three layers (Laddha, 2018), contour aware CNN to generate multiscale feature representation for dealing with wide shape variations and overlapped cells (Razzak and Naz, 2017), SegNet encoder-decoder comprising stacked convolutional layer, batch normalization, and ReLu activation function (Tran et al., 2018) as well as fuzzy-based systems with input parameters such as area, perimeter, and solidity of cells (Hiren and Velani, 2017; Shirazi et al., 2018; Macawile et al., 2018). Xie et al. (2018) proposed FCRN-A and FCRN-B (Fully Convolutional Regression Networks) for microscopic biomedical image analysis. Arbelle and Raviv (2018) introduced Rib-cage architecture for the discriminator part of adversarial neural network for microscopic image segmentation. Duggal et al. (2016) implemented a 4-layer deep belief network. Vijayalakshmi and Kanna (Vijayalakshmi et al., 2020) introduced the VGG19-SVM model as a transfer learning technique for biomedical image classification. Zhang et al. (2017) developed a variant of U-Net by replacing standard convolutional layers in the original U-Net with the deformable convolutional kernels. Some other variants of U-Net have also been presented in the literature in recent times (e.g., MultiResU-Net with the residual convolutional path between encoder-decoder (Ibtehaz and Rahman, 2020), U-Net++ with nested, dense skip pathways (Zhou et al., 2018), Attention U-Net with attention module attached with convolutional layers (Oktay et al., 2018), etc.). Wang et al. (2018) developed their network from randomly generated CNN models from convolutional blocks with a given range of hyper-parameters followed by PatternNet (Li et al., 2018) for model fusion and a softmax layer.

Hernández et al. (Hernández et al., 2018) implemented a Feature Pyramid Network (FPN) for segmentation and VGG-11 based network for cell counting.

1.2. Cell segmentation benchmark datasets

The dataset used by Sheng et al. (2020) for Lymphoma classification includes a total of 1326 images collected from Ruijing Hospital, Shanghai Jiaotong University School of Medicine. The dataset contains two types of slide images, namely, a single target cell and multiple target cell images. Images have a resolution of 360 × 363 pixels. The dataset contains Blast (465), Lymphoma (696), Lymphocyte (486), and some other (26) cells, i.e., a total of 1673 cells. Ma et al. (2020) used the BCCD public database. It contains 12,447 blood cell enhancement slide images with a cell type label (CSV). Cell images are divided into four different types of WBCs: eosinophils, lymphocytes, monocytes, and neutrophils.

One of the most widely used blood cell segmentation dataset is ALL-IDB. This is an acute lymphoblastic leukemia image database for image processing (Labati et al., 2011) comprising microscopic slides containing Acute Lymphoblastic Leukemia cells. This dataset has two versions (ALL-IDB1 & ALL-IDB2). ALL-IDB1 is used for segmentation and comprises 108 images of resolution 2592 × 1944. ALL-IDB2 is a classification dataset with 260 single cell images of resolution 257 × 257. On the other hand, the authors in (Shahzad et al., 2020; Salem et al., 2016) used the ALL-IDB1 dataset. Three datasets were used by Delgado-Ortet et al. (2020): dataset A consisting of 186 blood smear image slides of healthy cells of resolution 2400 × 1800 × 3, dataset B comprising 331 blood smear image slides of parasitized cells of resolution 2400 × 1800 × 3, and dataset C consisting of 27,558 images of masked and cropped individual erythrocytes. Dataset A and B do not provide segmentation mask. Raza et al. (2019) considered a number of datasets for segmentation of various objects in microscopy images. Datasets are as follows: (a) Warwick-QU dataset of 165 slide images published in GLand Segmentation (GLaS) challenge, (b) Computational precision medicine (CPM) dataset of 64 slide images first published as part of a challenge contest at Medical Image Computing and Computer-Assisted Interventions (MICCAI) 2017 and (c) a custom dataset of 10 slide images of size 2048 × 2048 pixels (11,163 Exocrine & Endocrine cells) captured by multiplexed fluorescence microscopes. Notably, the main challenges in the custom dataset used in Raza et al. (2019) include the variation in intensity levels of images and difficulty with separating neighboring cells.

In (Xie et al., 2018), Xie et al. used one synthetic and four real datasets for counting and detecting microscopic cells. The synthetic dataset (Lempitsky and Zisserman, 2010) contains images of cell nuclei on fluorescence microscopy generated with the algorithm proposed in (Lehmussola et al., 2007). It has 200 slide images of size 256 × 256, where each image has an average of 174 ± 64 cells. Among the four real datasets used by Xie et al., 3 are relevant to our study. These are: (a) retinal pigment epithelial (RPE) cell slide images obtained from 53 normal human donor eyes having age between 18.8 and 58.6 years with RPE cell count of 3, 556, 290 ±490, 700 (Panda-Jonas et al., 1996), (b) embryonic stem cells database of 92 slide images in Tagged Image File (.tif) format having a resolution of 1032 × 1040 pixels (Faustino et al., 2009), and (c) plasma cells slide images in bone marrow specimens obtained from 87 patients of whom 28 have multiple myeloma, 29 has monoclonal gammopathy, and 30 has reactive plasmocytosis (Went et al., 2006).

Arbelle and Raviv (2018) used the H1299 dataset consisting of 72 image frames of size 512 × 640 pixels. Each frame captures approximately 50 cells. Manual annotation of 15 randomly selected frames was

done by an expert. This segmentation dataset is annotated using three labels, namely, background (red), cell nucleus (green), and nucleus contour (blue). Duggal et al. (2016) used a dataset containing microscopic image slides from patients having B-Lineage acute lymphoblastic leukemia (ALL) for segmenting WBC blast nuclei. It consists of 51 images that are cropped from the stained slide images. Vijayalakshmi and Kanna (Vijayalakshmi et al., 2020) used only 100 slide samples collected from Tagore Medical College & Hospital and MAMIC database involving 100 infected subjects, which results in malaria image digital corpus (MIDC). It has a total of 2550 images, of which 1030 images are infected with P.falciparum and 1520 images are non-infected. Their work involved classification of infected and non-infected cells from blood smear image slides.

Zhang et al. (2017) used a dataset from UPMC (University of Pittsburgh Medical Center) for cell segmentation, which includes 32 raw microscopy slide images with resolution 1920 × 1080 × 4. For ease of computation, each image was divided into four parts and, each part was resized into a 256 × 256 pixel size. Thus, the trainable dataset contains 128 samples. Wang et al. (2018) used a publicly available dataset that has a collection of 410 slide images stained with Wright's stain, a mixture of eosin (red) and methylene blue dyes. These slide images have a resolution of 640 × 480 pixels. Their work involved WBC classification.

Hernández et al. (Hernández et al., 2018) used the BBBC005 dataset by Broad Institute's Bioimage Benchmark Collection (Ljosa et al., 2012), which contains 9,600 simulated microscopy images of cell body stained cells simulated using the SIMCEP simulation platform (Lehmussola et al., 2007). Slide images are of size 696 × 520 pixels encoded in the 8-bit Tagged Image File format. Of these 9,600 images, 600 images have a corresponding foreground mask for segmentation. Furthermore, all 9600 images have associated cell counts with an upper limit of 100. Madhloom et al. (2012) used 180 RGB blood smear image slides with resolution 2080 × 1544 that were collected from the University of Malaya Medical Center (UMMC) for lymphoblast segmentation. We summarize the existing datasets and their sample counts, label type, cell counts in Table 1.

Table 1
Datasets and its corressponding Sample size, Label type, Cell count.

Dataset	Sample size	Label type	Cell count
SJTUSM (Sheng et al., 2020)	1326	Object detection	Slide image
Synthetic data	200	Object detection	Slide image
RPE	53	Object detection	Slide image
ESC	92	Object detection	Slide image
PC (Xie et al., 2018)	87	Object detection	Slide image
BCCD (Ma et al., 2020)	12,447	Classification	Slide image
MIDC (Vijayalakshmi et al., 2020)	2550	Classification	Slide image
Slide images (Wang et al., 2018)	410	Classification	Slide image
ALL-IDB1	108	Segmentation	Slide image
ALL-IDB2 (Labati et al., 2011)	260	Classification	Single cell image
Dataset A	186	Segmentation	Slide image
Dataset B	331	Segmentation	Slide image
Dataset C (Delgado-Ortet et al., 2020)	27,558	Classification	Single cell image
Slide images (Duggal et al., 2016)	51	Segmentation	Slide image
Warwick-QU	165	Segmentation	Slide image
CPM	64	Segmentation	Slide image
Custom data (Raza et al., 2019)	10	Segmentation	Slide image
UPMC (Zhang et al., 2017)	128	Segmentation	Slide image
UMMC (Madhloom et al., 2012)	180	Segmentation	Slide image
H1299 (Arbelle and Raviv, 2018)	72	Partly segmentation (15 mask)	Slide image
BBBC005 (Hernández et al., 2018)	9,600	Partly segmentation (600 mask)	Slide image
BBBC041Seg (Ours)	**1,328**	Segmentation	Slide image

1.3. Motivation and contribution

The transition from manually hand-crafted features to automatic learning of hierarchical features from input images introduces the requirement for quality datasets. However, the number of samples in these datasets which have annotated segmentation mask is considerably limited. The performance of any deep learning model largely depends on the samples it is being trained on. As the quest for improving deep learning models goes on, models are getting complex and deeper in architecture. Deeper models need more data for training and convergence to an optimal minimum, which otherwise leads to the problem of over parametrization. This motivates some studies, which aim to generate synthetic data for the desired task. This, however, cannot replicate the real-world scenarios of microscopic objects to the fullest, particularly for the presence of different acquisition protocols and rare diseases. This aspect hinders the proper evaluation of deep learning models.

Thanks to digital imaging techniques for a plethora of raw images but for generating ground truth extensive manual labor is required. This labor comes at a cost of time and effort with mental toiling to determine ambiguous regions of stained cells. For example, as reported in (Ma et al., 2020), 12,447 blood cell enhancement images are available in BCCD public database, but they do not include corresponding segmentation masks. Such high acquisition cost, and additionally, the privacy concerns, which is a crucial issue in the context of medical datasets, often preclude the use/access of large and diverse medical imaging datasets, particularly on part of the researchers working in resource-limited settings. Thus, often researchers rely on semi-automatic annotation tools followed by manual curating to create ground truths. This resulted in segmentation masks that are sub-optimal in quality, whereas a gold standard annotation mask is needed for the optimal performance of a model. Moreover, homogeneous images such that only healthy cells or only infected cells are the main cause of overfitting and poor inference on unknown examples. Deep learning models work best on training images that are diverse in terms of classes, shapes, and intensities, etc.

All these motivated us to focus on preparing/curating an annotated/labeled dataset that is large and diverse enough compared to other datasets for the same task. This would enable further research in automatic feature extraction of medical images and evaluation of algorithms by reducing dependency on synthetic labeled images and sub-optimal semi-automatic annotation tools introduced for fast annotation. Furthermore, this will also address the issue of homogeneity among images by providing not only different blood constituents but also unrecognized objects floating in unaltered cell plasma.

With the above backdrop, in this paper, we present a cell segmentation dataset, BBC041Seg, which consists of ground truth masks of different cell types from more than 1300 microscopic exam slides. We provide annotated masks as ground truths for images taken from BBBC041v1 dataset (Ljosa et al., 2012), which is a publicly available object detection dataset. Furthermore, we also conduct a benchmark study using the BBC041Seg dataset leveraging both non-learning rules-based methods and recent deep learning-based state-of-the-art (SOTA) methods for automatic cell segmentation. The contribution of this paper can be summarized as follows.

1. We prepare and introduce BBBC041Seg, a cell segmentation dataset consisting of 1300+ images from BBBC041-v1 (Ljosa et al., 2012), and their cell segmentation masks as ground truth labels, which is significantly larger and more diverse than existing benchmark datasets.

2. We perform a series of controlled experiments by implementing both classical rule-based and deep learning state-of-the-art approaches and provide a comparative analysis using the proposed dataset.
3. We make the dataset publicly available to provide a platform for researchers to focus more on generalized cell segmentation methods that are more clinically acceptable. Dataset is available at https://github.com/Deponker/Blood-cell-segmentation-dataset.

2. Methods

2.1. Dataset annotation procedure

As has been mentioned above, we start with the BBBC041v1 dataset that contains images of microscopic blood smears. BBBC041v1 dataset (Ljosa et al., 2012) originally contains the bounding box coordinates for each cell, and the original references of cells have been used to identify the individual cells. We specifically choose this dataset as it contains a wide range of morphological variations (Ljosa et al., 2012). Since the task is simply to identify foreground from background, the annotation procedure has been carried out by non-medical experts. The annotation procedure is briefly described below also see (Fig. 1). The images in the BBBC041v1 dataset have multiple challenges, including clumped cells, distorted shape, unwanted substances, low contrast, etc. Moreover, the images in the dataset have been collected from different locations, making it comparatively more diverse. While annotating, we followed the 60 % rule as follows. We include a cell segmentation mask only if the shape of the cell is at least 60 % preserved, and this is done by majority voting (in case of a disagreement) among the annotators. The rationale behind this 60 % rule is that cropped cells will not provide enough shape information. We made a segmentation mask from each slide by removing the background. To separate clumped or cells with touching boundaries, the annotators reached a consensus to use a 4-pixel brush to cut through the clumped region. This consensus was necessary for consistency among images and not to lose much information. We also removed boundary cells that are not present in their full shape. Fig. 2 represents some examples of the dataset with their corresponding masks.

2.2. Rule based methods

2.2.1. Otsu's method

Otsu's method (Sha et al., 2016) is a method that finds optimal threshold intensity automatically that separates images into foreground and background. It is separated by maximizing the inter-class variance.

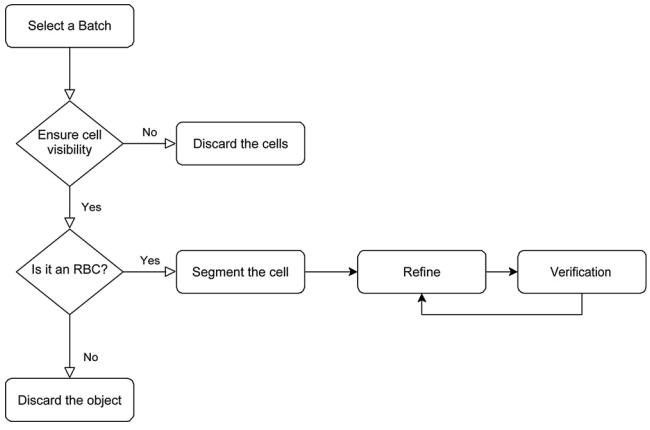

Fig. 1. Data annotation workflow. The refinement and verification steps were carried out through a majority voting scheme among the human annotators.

2.2.2. K-means clustering

K-means (Liu and Yu, 2009) method partitions a set of samples into *K* disjoint subsets where similar samples belong to the same subset. This is done by reducing the sum of the square criterion. For this work, we set the cluster value $K = 3$.

2.2.3. Balanced histogram thresholding (BHT)

BHT (Dos Anjos and Shahbazkia, 2008) is a histogram-based thresholding method where it is assumed that an image consists of two main classes: foreground and background. The goal of the method is to find the optimum threshold level by weighing the histograms and finally separating the two classes.

2.2.4. Marker-controlled watershed

Marker-controlled watershed transformations (Fan et al., 2019) have been suggested to mitigate the effects of extreme over-segmentation in the classical watershed algorithm. The over-segmentation caused by the existence of several local minima is the methods critical flaw. The marker controlled watershed transform is a region-growing approach that floods predefined markers onto a height map. Given an image, internal and external markers are extracted, followed by creating a modified gradient image. After that, the watershed transform floods the gradient image by dilating the markers simultaneously until colliding at watershed lines.

2.3. Deep learning methods

2.3.1. U-Net

U-Net (Ronneberger et al., 2015) architecture consists of an encoder and a decoder path. The encoder path contains several successive standard convolutional layers for feature extraction, followed by downsampling layers. The decoder path consists of a successive block of up-sampling layers followed by a convolutional layer. Moreover, U-net is symmetric, and each feature map generated in the contracting block is concatenated with the corresponding decoder block.

2.3.2. U-Net++

U-Net++ (Zhou et al., 2018) is similar to the original U-Net, except the encoder-decoder sub-networks are connected through a series of nested, dense skip pathways. This network was proposed to reduce the semantic gap between the two sub-networks in the original U-Net, where simple concatenation was applied. Therefore, U-Net++ is considered a more efficient design capable of better segmentation.

2.3.3. TernausNet

TernausNet (Iglovikov and Shvets, 2018) was developed to improve U-Net performance on various challenging datasets. Encoders in the original U-Net consist of 4 levels of downsampling for feature extraction. In TernausNet, the transfer learning technique is leveraged. It uses VGG11 (Simonyan and Zisserman, 2014) (i.e., 11 levels of downsampling for feature extraction) as an encoder with pre-trained weights from the ImageNet dataset (Krizhevsky et al., 2012) that contains 14 million hand-annotated images.

2.3.4. R2U-Net

R2U-Net (Alom et al., 2018) is a Recurrent Residual Convolutional Neural Network (RRCNN) based on the original U-Net architecture. Integration of residual block ensures better learning capability of a deep CNN. Similarly, for better semantic map generation, reduction in semantic gap is necessary; feature accumulation through recurrent block ensures that. Thus, R2U-Net outperforms standard U-Net on several datasets.

2.3.5. Attention U-Net

Attention U-Net (Oktay et al., 2018) implements attention gates (AGs) in the expanding path of U-Net model to filter the feature maps

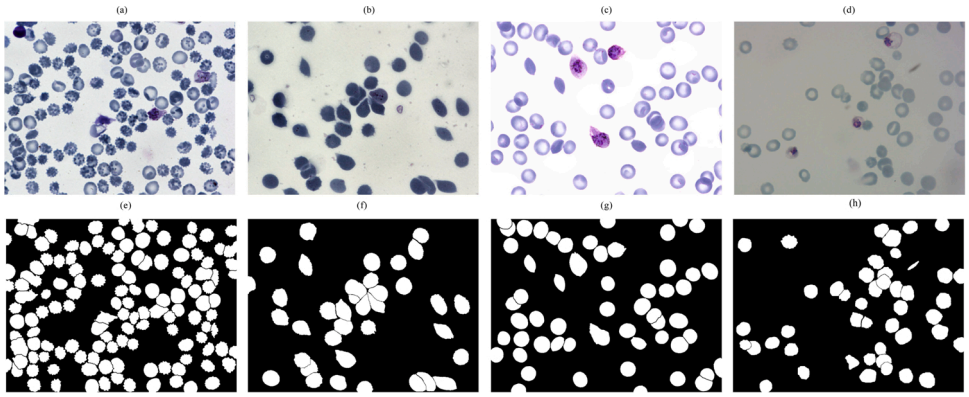

Fig. 2. Example of microscopic slides (a-d) with their corresponding segmentation masks (e-h) from the BBBC041Seg dataset.

propagated through the skip connections from the encoding path. U-Net model often suffers from dominant but irrelevant features in input images. AGs can implicitly suppress the learning of those features. Thus, network gets better at sensitivity and prediction accuracy.

2.3.6. Attention R2U-Net

As we can see that, R2U-Net is equipped with better feature extraction capabilities, and AGs can automatically suppress dominant irrelevant features in input images. We can leverage these powerful qualities by combining them in U-Net models. Thus, Attention R2U-Net (Das and Zhang, 2020) is created from the anticipation of better segmentation map generation.

2.3.7. Fully convolutional network

The Fully convolutional network (FCN) (Long et al., 2015) allows pixel-wise prediction instead of pathwise prediction, which provides better outputs. The last layer of the fully connected layer was replaced with a fully convolutional layer for pixel-wise prediction on an image. The translation invariance used in convolutional neural networks (CNNs) preserves the same information as inputs. The CNNs are built with convolution, pooling, and activation function. The architecture takes any arbitrary size of the input and produces an output of corresponding spatial dimensions. Finally, the multi-resolution layer simplifies the learning and inference rate. Therefore, the improved architecture allows multiple purposes of segmentation. The architecture of the network is presented in Fig. 3.

2.4. Evaluation metrics

We use Dice Coefficient and Jaccard Index as segmentation evaluation metrics. Jaccard Index is the intersection or overlap between the predicted mask and ground truth divided by the union or total area of predicted mask and ground truth. We compute Jaccard Index using Eq. 1 below.

$$Jacaard\ Index = \frac{\Sigma y\hat{y}}{\Sigma(y + \hat{y} - y\hat{y})} \tag{1}$$

Here, y and $\hat{y}$ refer to ground truth and predicted mask, respectively.

Dice Coefficient is twice the area of overlap or intersection between predicted mask and ground truth divided by the summation of the union and intersection of the predicted mask and ground truth. We compute Dice Coefficient using Eq. 2 below.

$$Dice = \frac{2\ \Sigma y\hat{y}}{\Sigma(y + \hat{y})} \tag{2}$$

Here symbols have the same meaning as in Eq. 1.

Jaccard Index and Dice Coefficient produce values ranging from 0 to 1. Values close to 0 indicate less similarity, whereas values close to 1 indicate more similarity between ground truth and predicted mask.

2.5. Code, data and experimental environment

The dataset is split into an 80:20 ratio for training and testing. Segmentation annotations have been done using GIMP. The experiments have been conducted on Google Colab using GPU in Python 3.7.7 with Tensorflow 2.4.1 and Keras backend 2.1.3. Codes are available at https://github.com/Deponker/Blood-cell-segmentation.

The dataset is available at https://github.com/Deponker/Blood-cell-segmentation-dataset.

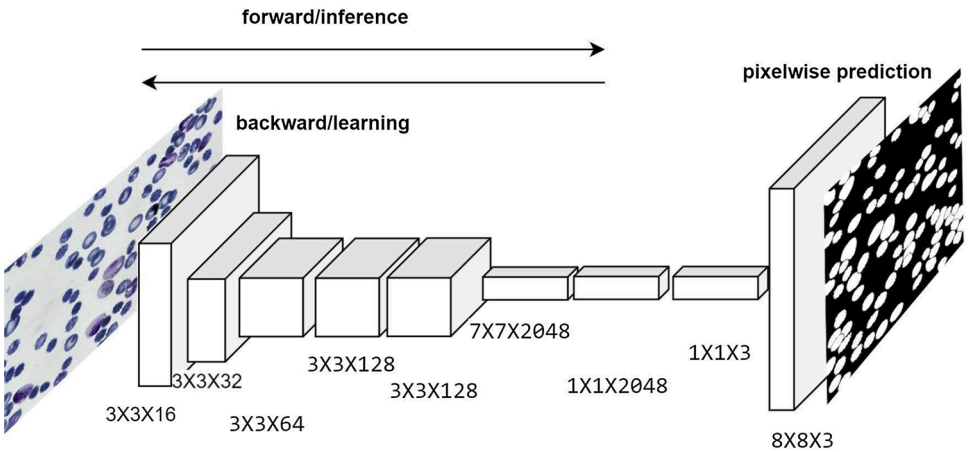

Fig. 3. Schematic of fully convolutional network architecture.

3. Results and discussion

We have benchmarked several celebrated segmentation methods on our proposed BBBC041Seg dataset that consists of 1,328 microscopic images. We consider both non-learning and learning based methods. For our deep learning-based experiments, we did not pre-process images and ran models for 20 epochs in a batch size of 1 with a validation set having 10 % of the available training data. Since our goal is to benchmark all these methods on our proposed dataset, we trained all the deep learning models without any additional hyperparameter tuning and data augmentations. The results are summarized in Table 2.

3.1. Learning based algorithms

TernausNet performed the highest score in terms of both Dice Coefficient (0.933) and Jaccard Index (0.8765) on the test set. Recall that, Ternausnet has the VGG11 encoder pre-trained on ImageNet. Despite an excellent score in both metrics, visual analysis reveals that TernausNet failed in some aspects while producing satisfactory segmentation maps for center region blood cells. For example, TernausNet could not distinguish between highly stained regions and actual cells. It produced a somewhat blurry result on these highly stained regions and considered them as a part of adjacent cells which is illustrated in Fig. 4(b) and marked using red boxes. It produced a segmentation map for cells that do not obey the 60 % rule and produced maps that are not completely white in terms of pixel colors. If the unwanted segmentation regions have complete white pixels rather than gray pixels, there would have been a drop in Dice and Jaccard Index due to more pixels being dissimilar.

U-Net also performed very well on our dataset and achieved a Dice Coefficient score of 0.930 and a Jaccard Index score of 0.871 compared to variants of U-Net, which were all trained from scratch. The visual analysis also revealed that U-Net performed well in terms of learning the 60 % rule. It produced a segmentation map for boundary cells in complete white pixels, which indicated the model's higher confidence. We hypothesize that as the 60 % rule does not include all cells at the boundary regions, U-Net has been penalized slightly for this confident behavior. In the case of stained regions, U-Net also suffered. It had difficulty distinguishing between stained regions and actual cells when highly stained regions and cells are identical in terms of pixel information.

Attention U-Net achieved a Dice Coefficient of 0.910 and a Jaccard Index score of 0.837. It is interesting to notice that there is a small difference between Dice and Jaccard scores for this model. We have observed that, with some exceptions in some regions, Attention U-Net was capable of learning the 60 % rule. However, this model introduced holes in the middle of segmented cells for very low contrast regions. These low contrast regions are often indistinguishable from the background pixels. It was a universal characteristic for Attention U-Net in our experiments. It failed to learn the phenomenon that occasionally found low contrast regions surrounded by high contrast regions are part of cells. In terms of stained regions, it merged those with adjacent cells, thereby producing distorted segmentation maps. Also, Attention U-Net could not segment clustered cells well, as these appeared as a segmentation mask of a large single cell.

U-Net++ achieved a Dice Coefficient score of 0.888 and a Jaccard Index score of 0.814. Though these scores reflect aggregate average on test set images, we have observed that U-Net++ was able to learn the 60 % rule. It produced quite satisfactory results at the boundary regions. This model also did well in terms of segmenting clustered cells, although it failed in stained regions miserably. For many instances, the model produced blurred outputs specifically for the stained regions. Sharp spiked edges from original images are also preserved in the predicted segmentation mask. Having more parameters, U-Net++ sometimes resulted in over-segmentation as compared to U-Net. Thus, it exhibited less generalization capability than U-Net. Both Dice Coefficient and Jaccard Index strongly penalized this behavior of U-Net++, which is also true for other deep learning models. For U-Net++ with deep supervision, Dice Coefficient and Jaccard Index scores degraded to 0.863, and 0.780 respectively. This configuration of U-Net++ seemed to have a difficulty of discarding boundary cells, as some amount of segmentation mask of boundary cells are visible. Though spiked edges are preserved, we have found that unwanted objects floating in the blood smear were segmented by this model. An example of this phenomenon is shown in Fig. 4(c). Such unwanted objects include dot-like floating substances which are not part of a cell. On a positive note, U-Net++ with deep supervision did not produce any holes in low contrast regions of cells. However, it still struggled to differentiate stained regions with cells, producing highly blurry segmentation maps in cell clusters.

R2U-Net achieved a Dice Coefficient of 0.867 and a Jaccard Index score of 0.777. We can see that these scores do not indicate very good segmentation performance in terms of the quality of the predicted mask as compared to previously mentioned models. By inspecting carefully, we found the presence of lower-level features in the output segmentation mask. We theorize that this could be due to the parameter-heavy and sophisticated architecture and zero fine-tuning on a moderate-size training set for the network. Other than that, R2U-Net appeared to learn the 60 % rule well while producing ambiguous segmentation maps for clustered cell regions. Characteristically important spiked edges in certain cells were also preserved but the model failed to distinguish between stained and actual cell regions.

FCN achieved 0.854 and 0.752 as the Dice Coefficient and Jaccard Index score, respectively. We observed that FCN produced quite an accurate segmentation mask in terms of pixel colors, cell clusters, and boundary cells, whereas the segmented cells' spatial features were disproportional with respect to the corresponding ground truths. This behavior resulted in high penalties when calculating Dice Coefficient and Jaccard Index scores.

Attention R2U-Net achieved a Dice score of 0.785 and a Jaccard Index score of 0.652. This complex and exotic network had lower-level features such as colors and textures in the output images. We hypothesize that this model particularly suffered from poor prediction due to convergence in a sub-optimal minimum in the absence of fine-tuning. Our top-performing model TernausNet has VGG11 encoder with weights from ImageNet, which was fine-tuned on our training dataset. Additionally, we experimented with U-Net, Attention U-Net and U-Net++ configuration. We implemented VGG16 encoder with weights from ImageNet for these three networks and then fine-tuned it on our training dataset. These networks achieved Dice Coefficient of 0.9337, 0.9261, 0.9148, and Jaccard Index scores of 0.8770, 0.8646, 0.8443, respectively. Three fine-tuned networks have improvements in Dice scores of about 0.29 %, 1.75 %, 5.78 %, and Jaccard Index of about 0.62 %, 3.22 %, 7.92 %, respectively. These experiments illustrate the superior effect of fine-tuning deep learning models and, we have observed that networks ranked last in terms of performance such as U-Net++ DL does considerably better when fine-tuned on our dataset. To further validate our hypothesis, segmentation masks from vanilla Attention

Table 2
Segmentation evaluation of different algorithm on test set.

Test set evaluation		
Method	Dice-coefficient	Jaccard Index
Otsu's method	92.60	86.50
BHT	52.50	49.48
Watershed	78.21	68.21
U-Net	93.09	87.16
U-Net++	88.80	81.44
TernausNet	**93.38**	**87.65**
R2U-Net	86.76	77.77
Attention U-Net	91.00	83.73
Attention R2U-Net	78.52	65.28
FCN	85.41	75.29

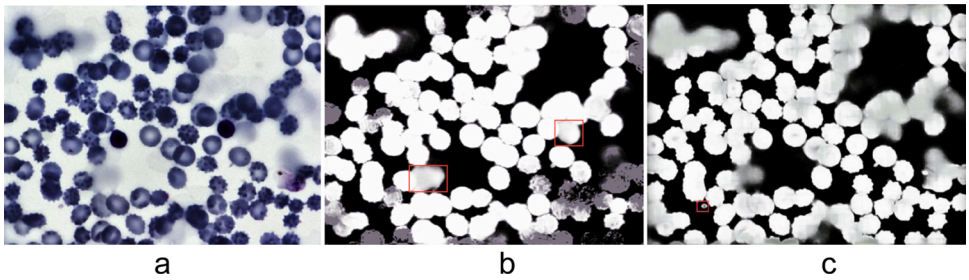

Fig. 4. (a) Original (b) Output of TernausNet, red bounding box indicates highly stained regions considered as cells (c) Output of U-Net++, red bounding box indicates unwanted objects.

R2U-Net were inspected carefully and, we found several indications of poor performance, such as spiked edges, clustered cells, stained regions were not distinguishable in the output images. Holes in the middle of cells were also present in segmented maps, although isolated cells had clear and distinguishable shapes in predicted segmentation masks. Both attention-based segmentation networks, such as Attention U-Net, and Attention R2U-Net had output images with some fuzzy boundary and, noise which were heavily penalized by our evaluation metrics.

3.2. Non-learning based algorithms

Otsu's thresholding method with blur achieved a Dice Coefficient score of 0.926 and a Jaccard Index score of 0.865, and without blur, the scores were almost identical: 0.925 and 0.864, respectively. Otsu demonstrated remarkable quantitative results in terms of both metrics. However, qualitatively, it performed poorly in some cases. Due to the low bimodality of histogram within the cell, the method generated segmentation masks with "holes" in the middle. The example of Otsu segmentation can be seen in Fig. 5. Also, as Otsu is a non-learning method, it does not differentiate between stains and cells while disobeying the 60 % rule. Poor qualitative performance despite a high score may largely be attributed to Otsu's hard thresholding ability. As ground truths are also hard-thresholded, the pixel similarity score is higher. Complete cell shapes and stain-free segmentation ensures superior qualitative analysis, whereas the Otsu method produced holes in the middle of cells, which has low intensity compared to the surrounding pixels. That also contributed to poor performance in segmentation.

K-mean thresholding achieved a Dice score of 0.933, and a Jaccard Index score of 0.879. Since both metrics compute similarly at a pixel level, it does not take into account complete or incomplete cell shapes (e.g., global context), stain, and unwanted substance-free segmentation. The reason for poor performance despite having good scores is attributed to the algorithm's inherent ability to threshold input images. In this case, the algorithm produced a hard thresholded segmentation mask, which gained a better pixel similarity score when compared to manually annotated hard thresholded ground truths. The absence of translation of input pixels to either 0 or 255 would penalize the algorithm heavily in terms of evaluation metrics. Another aspect of the poor performance of the algorithm is its learning ability. K-mean thresholding does not learn anything from input images, rather threshold images based on neighboring pixel intensity values. In the case of our dataset, cells often have low contrast, low intensity, and blurry boundaries because of applied stain and variability in cell's inherent absorption ability. So, it sometimes fails to segment those regions and produces incomplete cells with holes in the middle while segmenting high-intensity unwanted substances floating in cell plasma.

Balanced Histogram Thresholding (BHT) performed poorly with a Dice Coefficient of 0.525 and a Jaccard Index score of 0.494. The contrast in medical image modality was the main issue for this method. In some cases, due to low contrast and noisy images, BHT completely failed to produce any segmented mask.

The marker-controlled watershed algorithm achieved a Dice Coefficient score of 0.782 and a Jaccard Index score of 0.682. By visually inspecting the segmentation maps generated for the test set, we have found that watershed also failed to segment original images, for which contrast and pixel challenges exist. Predicted cell count is low for this method, along with the disadvantages of being a non-learning-based method.

4. Conclusion

In the area of medical image analysis, there are a plethora of algorithms compared to datasets available in the literature. By this research endeavor, we have tried to shorten the gap. We have contributed a large microscopic blood smear image dataset for cell segmentation and benchmarked various state-of-the-art algorithms on this dataset. Through our extensive experiment of implementing different algorithms, we reach an important conclusion that pre-trained networks with ImageNet weights are pretty useful in the case of blood cell segmentation dataset as we have achieved better performance scores by fine-tuning baseline networks. We acknowledge the limitation of implementing more algorithms and extend the dataset to an even bigger size. We intend to enlarge the sample size for this dataset to tens of thousands in the near future. Experimentation and achieving new benchmarks are open as future work on this dataset.

Authorship contributions

Category 1

A. Rahman, M.R.C. Mahdy, M.S. Rahman, H. Zunair: Conception and

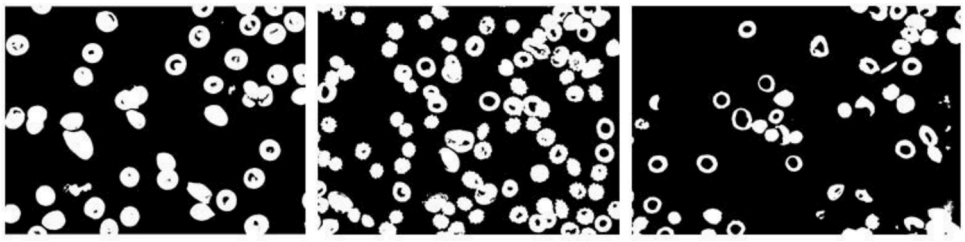

Fig. 5. Arbitrary output masks by OTSU method.

design of study.

A. Rahman, M.R.C. Mahdy: Acquisition of data.

D.S. Depto, S. Rahman, M.M. Hosen, M.S. Akter, T.R. Reme: Analysis and/or interpretation of data.

Category 2

A. Rahman, D.S. Depto, S. Rahman, M.M. Hosen, M.S. Akter, T.R. Reme, H. Zunair, M.S. Rahman, M.R.C. Mahdy: Drafting the manuscript.

M.S. Rahman, M.R.C. Mahdy, A. Rahman, H. Zunair, D.S. Depto: Revising the manuscript critically for important intellectual content.

Category 3

D.S. Depto, S. Rahman, M.M. Hosen, M.S. Akter, T.R. Reme, A. Rahman, H. Zunair, M.S. Rahman, M.R.C. Mahdy: Approval of the version of the manuscript to be published (the names of all authors must be listed):

Declaration of Competing Interest

The authors report no declarations of interest.

Acknowledgement

M.R.C Mahdy acknowledges the support of the NSU (North South University) internal grant: CTRGC grant 2019–20 and CTRGC grant 2020–21 (approved by the members of BOT, NSU, Bangladesh) and the support of TWAS international grant 2018 (Ref: 18-121 RG/PHYS/AS I-FR3240303643).

References

Algailani, H., Hamad, M.E.S., 2018. Detection of sickle cell disease based on an improved watershed segmentation. In: 2018 International Conference on Computer, Control, Electrical, and Electronics Engineering (ICC- CEEE). IEEE, pp. 1–4.

Al-Hafiz, F., Al-Megren, S., Kurdi, H., 2018. Red blood cell segmentation by thresholding and canny detector. Procedia Comp. Sci. 141, 327–334.

Alom, M.Z., Hasan, M., Yakopcic, C., Taha, T.M., Asari, V.K., 2018. Recurrent Residual Convolutional Neural Network Based on u-net (r2u-net) for Medical Image Segmentation arXiv preprint arXiv:1802.06955.

Alomari, Y.M., Sheikh Abdullah, S.N.H., Zaharatul Azma, R., Omar, K., 2014. Automatic detection and quantification of wbcs and rbcs using iterative structured circle detection algorithm. Comput. Math. Methods Med. 2014.

Arbelle, A., Raviv, T.R., 2018. Microscopy cell segmentation via adversarial neural networks. In: 2018 IEEE 15th International Symposium on Biomedical Imaging (ISBI 2018). IEEE, pp. 645–648.

Das, K., Zhang, Q., 2020. Convolutional Recurrent Residual u-net Embedded With Attention Mechanism and Focal Tversky Loss Function for Cancerous Nuclei Detection arXiv preprint arXiv:2010.04416.

Delgado-Ortet, M., Molina, A., Alférez, S., Rodellar, J., Merino, 2020. A deep learning approach for segmentation of red blood cell images and malaria detection. Entropy 22 (6), 657.

Dos Anjos, A., Shahbazkia, H.R., 2008. Bi-level image thresholding. Biosignals 2, 70–76.

Duggal, R., Gupta, A., Gupta, R., Wadhwa, M., Ahuja, C., 2016. Overlapping cell nuclei segmentation in microscopic images using deep belief networks. Proceedings of the Tenth Indian Conference on Computer Vision, Graphics and Image Processing 1–8.

Fan, Y., Beare, R., Matthews, H., Schneider, P., Kilpatrick, N., Clement, J., Claes, P., Penington, A., Adamson, C., 2019. Marker-based watershed transform method for fully automatic mandibular segmentation from cbct images. Dentomaxillofacial Radiology 48 (2), 20180261.

Faustino, G.M., Gattass, M., Rehen, S., de Lucena, C.J., 2009. Automatic embryonic stem cells detection and counting method in fluorescence microscopy images. In: 2009 IEEE International Symposium on Biomedical Imaging: From Nano to Macro. IEEE, pp. 799–802.

Ford, J., 2013. Red blood cell morphology. Int. J. Lab. Hematol. 35, 03.

Ghane, N., Vard, A., Talebi, A., Nematollahy, P., 2017. Segmentation of white blood cells from microscopic images using a novel combination of k-means clustering and modified watershed algorithm. J. Med. Signals Sens. 7 (2), 92.

Ghosh, P., Bhattacharjee, D., Nasipuri, M., 2016. Blood smear analyzer for white blood cell counting: a hybrid microscopic image analyzing technique. Applied Soft Computing 46, 629–638.

Hamouda, A., Khedr, A.Y., Ramadan, R.A., 2012. Automated red blood cell counting. Int. J. Comput. Sci. 1.

Hernández, C.X., Sultan, M.M., Pande, V.S., 2018. Using Deep Learning for Segmentation and Counting Within Microscopy Data arXiv preprint arXiv:1802.10548.

Hiren, D.V., Velani, N., 2017. An automated blood cell segmentation using fuzzy based system. In: 2017 8th International Conference on Computing, Communication and Networking Technologies (ICCCNT). IEEE, pp. 1–5.

Ibtehaz, N., Rahman, M.S., 2020. Multiresunet: rethinking the u-net architecture for multimodal biomedical image segmentation. Neural Netw. 121, 74–87.

Iglovikov, V., Shvets, A., 2018. Ternausnet: U-net With vgg11 Encoder Pre-trained on Imagenet for Image Segmentation arXiv preprint arXiv:1801.05746.

Jiang, K., Liao, Q.-M., Dai, S.-Y., 2003. A novel white blood cell segmentation scheme using scale-space filtering and watershed clustering. In: Proceedings of the 2003 International Conference on Machine Learning and Cybernetics (IEEE Cat. No. 03EX693), vol. 5. IEEE, pp. 2820–2825.

Krizhevsky, A., Sutskever, I., Hinton, G.E., 2012. Imagenet classification with deep convolutional neural networks. Adv. Neural Inform. Proce. Syst. 25, 1097–1105.

Labati, R.D., Piuri, V., Scotti, F., 2011. All-idb: the acute lymphoblastic leukemia image database for image processing. In: 2011 18th IEEE International Conference on Image Processing. IEEE, pp. 2045–2048.

Laddha, S.V., 2018. Analysis of White Blood Cell Segmentation Techniques and Classification Using Deep Convolutional Neural Network for Leukemia Detection.

Lehmussola, A., Ruusuvuori, P., Selinummi, J., Huttunen, H., Yli-Harja, O., 2007. Computational framework for simulating fluorescence microscope images with cell populations. IEEE Trans. Med. Imaging 26 (7), 1010–1016.

Lempitsky, V., Zisserman, A., 2010. Learning to count objects in images. Adv. Neural Inform. Proce. Syst. 23, 1324–1332.

Li, H., Ellis, J.G., Zhang, L., Chang, S.-F., 2018. Patternnet: visual pattern mining with deep neural network. Proceedings of the 2018 ACM on International Conference on Multimedia Retrieval 291–299.

Liao, Q., Deng, Y., 2002. An accurate segmentation method for white blood cell images. In: Proceedings IEEE International Symposium on Biomedical Imaging. IEEE, pp. 245–248.

Liu, D., Yu, J., 2009. Otsu method and k-means. In: 2009 Ninth International Conference on Hybrid Intelligent Systems, 1. IEEE, pp. 344–349.

Ljosa, V., Sokolnicki, K.L., Carpenter, A.E., 2012. Annotated high-throughput microscopy image sets for validation. Nat. Methods 9 (7), pp. 637–637.

Long, J., Shelhamer, E., Darrell, T., 2015. Fully convolutional networks for semantic segmentation. Proceedings of the IEEE Conference on Computer Vision and Pattern Recognition (CVPR). June.

Ma, L., Shuai, R., Ran, X., Liu, W., Ye, C., 2020. Combining dc-gan with resnet for blood cell image classification. Medical & Biological Engineering & Computing, pp. 1–14.

Macawile, M.J., Quiñones, V.V., Ballado, A., Cruz, J.D., Caya, M.V., 2018. White blood cell classification and counting using convolutional neural network. In: 2018 3rd International Conference on Control and Robotics Engineering (ICCRE). IEEE, pp. 259–263.

Madhloom, H.T., Kareem, S.A., Ariffin, H., 2012. An image processing application for the localization and segmentation of lymphoblast cell using peripheral blood images. J. Med. Syst. 36 (4), 2149–2158.

Makkapati, V.V., Rao, R.M., 2009. Segmentation of malaria parasites in peripheral blood smear images. In: 2009 IEEE International Conference on Acoustics, Speech and Signal Processing. IEEE, pp. 1361–1364.

Mandal, S., Kumar, A., Chatterjee, J., Manjunatha, M., Ray, K., 2010. Segmentation of blood smear images using normalized cuts for detection of malarial parasites. In: 2010 Annual IEEE India Conference (INDICON). IEEE, pp. 1–4.

Moallem, G., Poostchi, M., Yu, H., Silamut, K., Palaniap- pan, N., Antani, S., Hossain, M. A., Maude, R.J., Jaeger, S., Thoma, G., 2017. Detecting and segmenting white blood cells in microscopy images of thin blood smears. In: 2017 IEEE Applied Imagery Pattern Recognition Workshop (AIPR). IEEE, pp. 1–8.

Mohammed, E.A., Mohamed, M.M., Naugler, C., Far, B.H., 2013. Chronic lymphocytic leukemia cell segmentation from microscopic blood images using watershed algorithm and optimal thresholding. In: 2013 26th IEEE Canadian Conference on Electrical and Computer Engineering (CCECE. IEEE, pp. 1–5.

Mohapatra, S., Patra, D., Satpathi, S., 2010. Image analysis of blood microscopic images for acute leukemia detection. In: 2010 International Conference on Industrial Electronics, Control and Robotics. IEEE, pp. 215–219.

Mohapatra, S., Patra, D., Kumar, K., 2011. Blood microscopic image segmentation using rough sets. In: 2011 International Conference on Image Information Processing. IEEE, pp. 1–6.

Nasir, A.A., Mashor, M., Mohamed, Z., 2012. Segmentation based approach for detection of malaria parasites using moving k-means clustering. In: 2012 IEEE-EMBS Conference on Biomedical Engineering and Sciences. IEEE, pp. 653–658.

Nawa, K., Suryani, E., Prasetyo, H., 2019. Dengue virus infected leukocyte classification on microscopic images with image histogram based support vector machine. In: 2019 5th International Conference on Science and Technology (ICST), vol. 1. IEEE, pp. 1–5.

Nierhaus, A., Klatte, S., Linssen, J., Eismann, N.M., Wichmann, D., Hedke, J., Braune, S. A., Kluge, S., 2013. Revisiting the white blood cell count: immature granulocytes count as a diagnostic marker to discriminate between sirs and sepsis-a prospective, observational study. BMC Immunol. 14 (1), 8.

Oktay, O., Schlemper, J., Folgoc, L.L., Lee, M., Heinrich, M., Misawa, K., Mori, K., McDonagh, S., Hammerla, N.Y., Kainz, B., et al., 2018. Attention u-net: Learning Where to Look for the Pancreas arXiv preprint arXiv:1804.03999.

Panda-Jonas, S., Jonas, J.B., Jakobczyk-Zmija, M., 1996. Retinal pigment epithelial cell count, distribution, and correlations in normal human eyes. Am. J. Ophthalmol. 121 (2), 181–189.

Raza, S.E.A., Cheung, L., Shaban, M., Graham, S., Epstein, D., Pelengaris, S., Khan, M., Rajpoot, N.M., 2019. Micronet: a unified model for segmentation of various objects in microscopy images. Med. Image Anal. 52, 160–173.

Razzak, M.I., Naz, S., 2017. Microscopic blood smear segmentation and classification using deep contour aware cnn and extreme machine learning. In: 2017 IEEE Conference on Computer Vision and Pattern Recognition Workshops (CVPRW). IEEE, pp. 801–807.

Ronneberger, O., Fischer, P., Brox, T., 2015. U-net: convolutional networks for biomedical image segmentation. In: International Conference on Medical Image Computing and Computer-Assisted Intervention. Springer, pp. 234–241.
Sadeghian, F., Seman, Z., Ramli, A.R., Kahar, B.H.A., Saripan, M.-I., 2009. A framework for white blood cell segmentation in microscopic blood images using digital image processing. Biol. Proced. Online 11 (1), 196.
Salem, N., Sobhy, N.M., El Dosoky, M., 2016. A comparative study of white blood cells segmentation using otsu threshold and watershed transformation. J. Biomed. Eng. Med. Imaging 3 (3), pp. 15–15.
Savkare, S., Narote, S., 2015. Blood cell segmentation from microscopic blood images. In: 2015 International Conference on Information Processing (ICIP). IEEE, pp. 502–505.
Savkare, S., Narote, A., Narote, S., 2016. Automatic blood cell segmentation using k-mean clustering from microscopic thin blood images. Proceedings of the Third International Symposium on Computer Vision and the internet 8–11.
Sha, C., Hou, J., Cui, H., 2016. A robust 2d otsu's thresholding method in image segmentation. J. Visual Commun. Image Representation 41, 339–351.
Shahzad, M., Umar, A.I., Khan, M.A., Shirazi, S.H., Khan, Z., Yousaf, W., 2020. Robust method for semantic segmentation of whole-slide blood cell microscopic images. Comput. Math. Methods Med. 2020.
Sharif, J.M., Miswan, M., Ngadi, M., Salam, M.S.H., bin Abdul Jamil, M.M., 2012. Red blood cell segmentation using masking and watershed algorithm: a preliminary study. In: 2012 International Conference on Biomedical Engineering (ICoBE). IEEE, pp. 258–262.
Sheng, B., Zhou, M., Hu, M., Li, Q., Sun, L., Wen, Y., 2020. A blood cell dataset for lymphoma classification using faster r-cnn. Biotechnol. Biotechnolog. Equip. 34 (1), 413–420.
Shirazi, S.H., Umar, A.I., Haq, N., Naz, S., Razzak, M.I., Zaib, A., 2018. Extreme learning machine based microscopic red blood cells classification. Cluster Comput. 21 (1), 691–701.
Simonyan, K., Zisserman, A., 2014. Very Deep Convolutional Networks for Large-scale Image Recognition arXiv preprint arXiv:1409.1556.
Sundara, S.M., Aarthi, R., 2019. Segmentation and evaluation of white blood cells using segmentation algorithms. In: 2019 3rd International Conference on Trends in Electronics and Informatics (ICOEI). IEEE, pp. 1143–1146.
Tran, T., Kwon, O.-H., Kwon, K.-R., Lee, S.-H., Kang, K.-W., 2018. Blood cell images segmentation using deep learning semantic segmentation. In: 2018 IEEE International Conference on Electronics and Communication Engineering (ICECE). IEEE, pp. 13–16.
Vijayalakshmi, A., et al., 2020. Deep learning approach to detect malaria from microscopic images. Multimed. Tools Appl. 79 (21), 15297–15317.
Vromen, J., McCane, B., 2006. Red Blood Cell Segmentation Using Guided Contour Tracing.
Wang, J.L., Li, A.Y., Huang, M., Ibrahim, A.K., Zhuang, H., Ali, A.M., 2018. Classification of white blood cells with patternnet-fused ensemble of convolutional neural networks (pecnn). In: 2018 IEEE International Symposium on Signal Processing and Information Technology (ISSPIT). IEEE, pp. 325–330.
Went, P., Mayer, S., Oberholzer, M., Dirnhofer, S., 2006. Plasma cell quantification in bone marrow by computer-assisted image analysis. Histology and Histopathology.
Xie, W., Noble, J.A., Zisserman, A., 2018. Microscopy cell counting and detection with fully convolutional regression networks. Comput. Methods Biomech. Biomed. Eng. Imaging Vis. 6 (3), 283–292.
Zhang, C., Xiao, X., Li, X., Chen, Y.-J., Zhen, W., Chang, J., Zheng, C., Liu, Z., 2014. White blood cell segmentation by color-space-based k-means clustering. Sensors 14 (9), 16128–16147.
Zhang, M., Li, X., Xu, M., Li, Q., 2017. Image Segmentation and Classification for Sickle Cell Disease Using Deformable u-net arXiv preprint arXiv:1710.08149.
Zhou, Z., Siddiquee, M.M.R., Tajbakhsh, N., Liang, J., 2018. Unet++: a nested u-net architecture for medical image segmentation. Deep Learning in Medical Image analysis and Multimodal Learning for Clinical Decision Support. Springer, pp. 3–11.